Inverse Designed THz Spectral Splitters

Sourangsu Banerji, *Student Member, IEEE*, Yu Shi, *Student Member, IEEE*, Vivian Song-En Su, *Student Member, IEEE*, Udayan Ghosh, *Student Member, IEEE*, Jacqueline Cooke, *Student Member, IEEE*, Yong Lin Kong, *Member, IEEE*, Lei Liu, *Senior Member, IEEE*, and Berardi Sensale-Rodriguez, *Senior Member, IEEE*

***Abstract*— This letter reports proof-of-principle demonstration of 3-D printable, low-cost, and compact terahertz (THz) spectral splitters based on diffractive optical elements (DOEs) designed to disperse incident collimated broadband THz radiation (0.5–0.7 THz) at a prespecified distance. Via inverse design, we show that it is possible to design a diffractive optic that can split broadband incident spectrum in any desired fashion, as is evidenced from both finite-difference time domain (FDTD) simulations and measured intensity profiles using a 500–750-GHz vector network analyzer (VNA). Due to its straightforward as well as simple construction without the usage of movable parts, our approach, in principle, can have various applications such as in portable, low-cost spectroscopy as well as in wireless THz communication systems as a THz demultiplexer.**

***Index Terms*— Diffractive optics, inverse design, spectral splitter.**

I. Introduction

SPECTROMETERS are widely used in optical characterization, chemical analysis, etc. [1], [2]. Traditional spectrometers harness gratings (typically one for each blazing wavelength or multiorders) or prisms, coupled with other mechanical and electronic parts, to disperse and detect the incident spectrum [1]. The necessity to assemble multiple components within a single system renders them bulky, sensitive to alignment, and suffering from low throughput due to crosstalk. Hence, they are not the optimal choices for broad commercial and industrial applications, where small footprint and simple hardware are required [2]. From such a perspective, coded apertures have been previously developed to construct compact computational spectrometers over both visible [3], [4] and infrared [5] regimes. However, such an approach is limited to narrow spectral bands and sensitive to noise.

Nonetheless, from a computational perspective, we can show that a single broadband diffractive optic can be inverse designed via numerical optimization of the structure's surface topology to split the incident broadband radiation under arbitrary splitting conditions. This inverse design formulation is employed extensively in digital holography [6]–[10], where a hologram is designed to project a predefined intensity pattern allowing the phase in the image plane to be arbitrary, i.e., "*phase as a free parameter*" [11].

Manuscript received January 26, 2021; accepted March 8, 2021. Date of publication March 12, 2021; date of current version May 10, 2021. This work was supported in part by the NSF under Award ECCS #1936729, Award MRI #1828480, and Award EFRI #1830958 and in part by the Air Force Office of Scientific Research (AFOSR) under Award FA9550-18-1-033. *(Corresponding author: Sourangsu Banerji.)*

Sourangsu Banerji, Jacqueline Cooke, and Berardi Sensale Rodriguez are with the Department of Electrical and Computer Engineering, University of Utah, Salt Lake City, UT 84108 USA (e-mail: sourangsu.banerji@utah.edu).

Yu Shi and Lei Liu are with the Department of Electrical Engineering, University of Notre Dame, Notre Dame, IN 46556 USA.

Vivian Song-En Su, Udayan Ghosh, and Yong Lin Kong are with the Department of Mechanical Engineering, University of Utah, Salt Lake City, UT 84108 USA.

Color versions of one or more figures in this letter are available at https://doi.org/10.1109/LMWC.2021.3065657.

Digital Object Identifier 10.1109/LMWC.2021.3065657

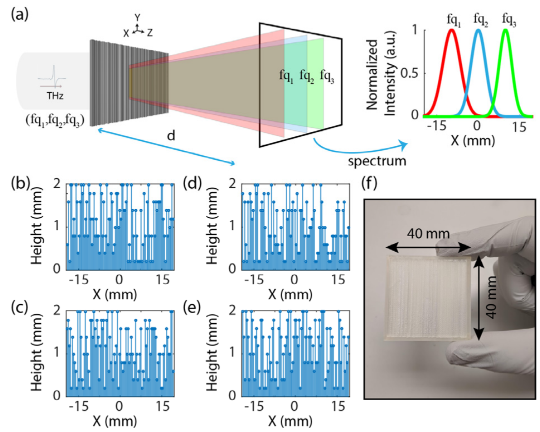

Fig. 1. (a) Schematic of the spectral splitter with a splitting distance $d = [35$ and 50 cm$]$ under broadband illumination ($\lambda_1 = 0.6$ mm [0.5 THz], $\lambda_2 = 0.5$ mm [0.6 THz], and $\lambda_3 = 0.4$ mm [0.7 THz]). The designed structure splits the incoming THz wave into a series of spatially separated lines at the prespecified design distance. (b)–(e) Pixel height distribution for the spectral splitter with a maximum pixel height of 2 mm. The dimensions (length and width) of the spectral splitter were 40 mm. (f) Optical micrograph of a fabricated sample.

In previous work, we have numerically demonstrated that designing splitters to split incident broadband terahertz (THz) radiation spatially is possible [12], [13]. In this letter, we extend this to experimentally demonstrate four spectral splitters with the help of geometric optimization of heights of each individual element ("pixel") within the diffractive optic for a broadband THz spectrum, i.e., from 0.5 to 0.7 THz. Unlike conventional structures, such as gratings, the splitters described in this work can arbitrarily disperse at predefined arbitrary spatial locations. The use of 3-D printing renders a simple and cost-effective solution as evidenced from previous diffractive structures shown in [14] and [15].

II. Methods

A. Design

From a fundamental standpoint, the idea behind designing a splitter structure [Fig. 1(a)] is related to inverse scattering. Therefore, optimization is a suitable approach for choosing an appropriate surface topography to attain desired functionality. Details of the optimization technique employed here, which is based on a gradient descent assisted binary search, have been provided in our earlier works [12], [13], [16], and [17]. Regardless of the particular algorithm employed for optimization, the two key metrices that guide the inverse design are (1) choice of an appropriate target function during the initiation of the optimization algorithm and (2) suitable Figure of Merit (FoM) function to enable a convergent solution. In this work, the target function (T_i) was defined as a Gaussian function with full-width-at-half-maximum (FWHM), and W_i determined by the far-field diffraction limit. That is

$$T_i\left(x'\right) = \exp\left\{-\frac{\left[x' - x'_{fq_i}\right]^2}{\left(2 * W_i\right)^2}\right\} \tag{1}$$

where x' denotes spatial position and x'_{fqi} denotes the spatial location at which intensity peaks in the observation plane for each frequency sample. The FoM was defined as

$$\text{FoM} = \frac{\sum_{i=1}^{N}\omega_i\theta_i}{N} - 10\frac{\sum_{i=1}^{N}\omega_i\varphi_i}{N} \tag{2}$$

where the first and the second terms in (2) describe the average weighted efficiency θ_i and the weighted normalized absolute difference φ_i over N wavelength samples is written as

$$\theta_i = \frac{\int_{x_{\min'}}^{x_{\max'}} I_i\left(x'\right)T_i\left(x'\right)dx'}{\int_{x_{\min'}}^{x_{\max'}} I_i(x')dx'} \tag{3}$$

$$\varphi_i = \frac{\int_{x_{\min'}}^{x_{\max'}} |\text{Norm}(I_i\left(x'\right)) - T_i\left(x'\right)|dx'}{\int_{x_{\min'}}^{x_{\max'}} dx'}. \tag{4}$$

The term $I_i(x')$ denotes the simulated intensity distribution function and $T_i(x')$ is the designated target function for the ith frequency sample. $x'_{\min}$ and $x'_{\max}$ are the limits of integration spanning from the leftmost to the rightmost in these structures. ω_i denotes the weighting coefficient which was fixed at 0.99 in the designed structures. The optimization and simulation of the structures were done using custom-made MATLAB code and Lumerical finite-difference time domain (FDTD) solutions, respectively.

The dimensions of the splitter were taken to be 40 mm by 40 mm in length and width, respectively. The structure consisted of multilevel pixels having maximum thickness $h_{\max} = 2000\ \mu$m, minimum thickness $h_{\min} = 200\ \mu$m, and height level step $\Delta h = 200\ \mu$m; which sets the number of distinct height levels (P) to $P = 10$. The pixels have a width $w = 400\ \mu$m; which sets the number of pixels, i.e., $N = 200$. The THz spectral splitters were designed to split the incident broadband radiation at a distance d = [35 and 50 mm]. In total, four different spectral splitters were designed to portray the robust and dynamic splitting capability of our inverse designed-based formulation. Fig. 1(b)–(e) depicts the pixel height profile along with relevant geometric dimensions for all the designs.

Polylactic acid (PLA) was taken as the design material for the splitters. Refractive index and extinction coefficient were taken based on the values measured in our previous work [18]. Other materials like polystyrene have an overall lower absorption in this frequency range [19] but are not 3-D printable at our current facilities.

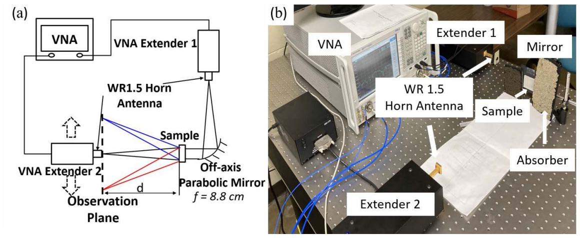

Fig. 2. (a) Schematic and (b) experimental setup used to characterize the THz spectral splitters.

B. Fabrication

A 3-D CAD model of THz spectral was first created with optimized pixel height and the model was 3-D printed (Ultimaker 3) with PLA filament as shown in Fig. 1(f).

C. Measurement

The spectral splitter was experimentally characterized in a free space quasi-optical THz measurement system (as shown in Fig. 2), including an Agilent N5245A vector network analyzer (VNA) with two WR-1.5 bands (500–750 GHz) frequency extenders. The two ports were first calibrated using Short-Open-Load-Through (SOLT) technique before the free space measurements. For the purpose of this measurement, the incident electromagnetic (EM) wave was generated by port 1 of the VNA and provided through a WR-1.5 diagonal horn antenna (provided by Virginia Diodes, Inc.). The E-plane of the antenna was aligned with yz plane of the splitter [see Fig. 1(a)], in accordance with simulation. The THz beam, which was collimated by an off-axis parabolic mirror (focal length f = 8.8 cm), can then be approximately treated as a plane wave. The beam waist (w_0) was measured to be 31.5 mm (radius) after the parabolic mirror so that the incoming THz beam can illuminate the entire sample area (40 mm × 40 mm). An absorber was placed around the sample to minimize the interference by shielding the surrounding EM wave. The S-parameters were then measured along the observation plane at a distance "d" from the sample and the corresponding transmitted power was collected. The amplitudes of the transmitted power spectrum were obtained directly from raw measurements and then normalized to the peak value of each beam at designed frequency (i.e., 0.5, 0.6, and 0.7 THz). For samples 1 and 2, the transmitted power spectrum was obtained at d = 35 cm, whereas d becomes 50 cm for samples 3 and 4.

III. Results and Discussion

Figs. 3(a) and (b) and 4(a) and (b), respectively, depict the simulated and measured spectral maps of two spectral splitters that were designed to split incident THz frequencies in a regular sequence (gradual split) across the observation plane at a predetermined distance of 35 and 50 cm for the designed frequencies of 0.5, 0.6, and 0.7 THz. In addition to this, Figs. 3(c) and (d) and 4(c) and (d) portray the simulated and measured spectral maps of a separate set of two more spectral splitter designs that were designed to split the

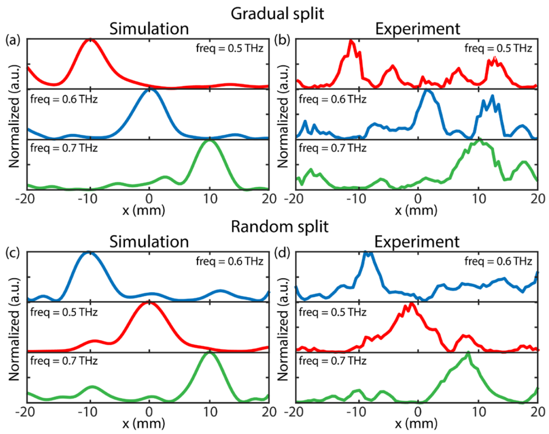

Fig. 3. Spectral splitter designs for a gradual split (sample 1 and sample 2) with (a) simulated and (b) measured spectral map at a splitting distance $d = 35$ cm under broadband illumination ($\lambda_1 = 0.6$ mm [0.5 THz], $\lambda_2 = 0.5$ mm [0.6 THz], and $\lambda_3 = 0.4$ mm [0.7 THz]). The corresponding spectral splitter designs for a random split (c) simulated and (d) measured spectral map at a splitting distance $d = 35$ cm under broadband illumination ($\lambda_1 = 0.5$ mm [0.6 THz], $\lambda_2 = 0.6$ mm [0.5 THz], and $\lambda_3 = 0.4$ mm [0.7 THz]).

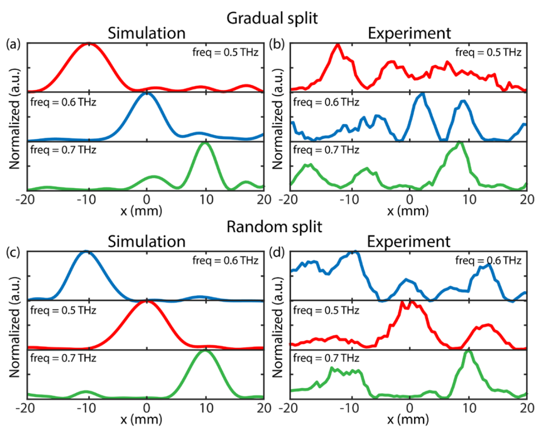

Fig. 4. Spectral splitter designs for a gradual split (sample 3 and sample 4) with (a) simulated and (b) measured spectral map at a splitting distance $d = 50$ cm under broadband illumination ($\lambda_1 = 0.6$ mm [0.5 THz], $\lambda_2 = 0.5$ mm [0.6 THz], and $\lambda_3 = 0.4$ mm [0.7 THz]). The corresponding spectral splitter designs for a random split (c) simulated and (d) measured spectral map at a splitting distance $d = 50$ cm under broadband illumination ($\lambda_1 = 0.5$ mm [0.6 THz], $\lambda_2 = 0.6$ mm [0.5 THz], and $\lambda_3 = 0.4$ mm [0.7 THz]).

same incident THz radiation in an arbitrary sequence (random split) across the observation plane at a predetermined distance of 35 cm [Fig. 3(c) and (d)] and 50 cm [Fig. 4(c) and (d)] subsequently. In general, from the spectral plots of both Figs. 3 and 4, it is evident that the split does happen even though the exact spatial location might be a bit off in the measured spectral profile.

This can be attributed to the following: under alike geometric conditions, spectral resolution offered by the nonregular-sequence design tends to be higher than that by the design with regular spectral split due to the spectral correlation function. In principle, the spectral correlation function measures how similar the diffraction patterns are at two distinct wavelengths. For regular-sequence spectral splitter designs, the spatial–spectral map changes relatively smoothly in contrast to that of a random design, which often experiences abrupt variations. Therefore, the correlation function for random designs becomes narrower, which makes it easier to distinguish between frequencies. These observations are consistent with those of earlier works reported in the literature for such diffractive optic-based splitter designed at optical frequencies [20]–[22].

However, here an important observation can be made. The splitter designs, which had a random non-monotonic split of the incident THz frequencies, depicted relatively better performance than their regular-sequence counterparts. In general, samples 2 and 4 have a clean spectral map with suppressed side lobes with respect to both sample 1 and sample 3. In fact, one can observe that sample 2 has the best split performance among all the four designs.

In addition to the spectral map, the amplitude of the THz beam and, hence, the loss performance of the splitter were analyzed. The raw data showed that the amplitudes of the diffractive beams vary in different measurements, but the loss of the proposed splitter, which is mainly from the dielectric loss of the material with a complex refractive index, was estimated to be around 12 dB in all cases. Although this loss is relatively larger than that reported in some other works, e.g., [23], [24], our results demonstrate the effectiveness of the proposed design principle with a freeform fabrication approach using 3-D printing. In the future, the loss can be lowered by employing materials with lower absorption (e.g., polystyrene).

Finally, the appearance of substantial side lobes in the measured results can be attributed to two reasons: (1) imperfection in fabrication due to the inherent limitation of 3-D printing (resolution $\sim$20 μm in [z] and $\sim$400 μm in [x, y]) and (2) imperfection in the measurement setup. A theoretical statistical study was already conducted on a very similar structure, i.e., a multilevel diffractive lens in [17] to showcase how the performance of the multilevel structure degrades with the inherent imperfection of fabrication, i.e., error in height and width of each pixel as well as density variations leading to index nonuniformities; and hence, a detailed discussion is omitted here. From the measurement perspective, the receiver VNA extender was manually moved along the desired plane, which will introduce additional misalignment errors. Besides, the receiver WR1.5 horn antenna is not a perfect point detector. Instead, its radiation pattern is also a Gaussian beam with certain beamwidth and substantial side lobes, which may broaden the main lobe and introduce side lobes in the measurements.

IV. Conclusion

In conclusion, we have demonstrated compact THz spectral splitters via inverse design which is capable of splitting incident broadband THz waves in free space with appreciable accuracy. Barring the challenges associated with the current state-of-the-art 3-D printing technology and the usage of better measurement facilities, this simple straightforward proof-of-concept demonstration of such spectral splitters evidences the fact that the proposed structures can be crucial in enabling portable, low-cost spectrometers as well as in wireless communications as THz demultiplexers.

REFERENCES

[1] C. P. Bacon, Y. Mattley, and R. DeFrece, "Miniature spectroscopic instrumentation: Applications to biology and chemistry," *Rev. Sci. Instrum.*, vol. 75, no. 1, pp. 1–16, Jan. 2004.

[2] M. Khorasaninejad, W. T. Chen, J. Oh, and F. Capasso, "Super-dispersive off-axis meta-lenses for compact high resolution spectroscopy," *Nano Lett.*, vol. 16, no. 6, pp. 3732–3737, Jun. 2016.

[3] M. E. Gehm, S. T. McCain, N. P. Pitsianis, D. J. Brady, P. Potuluri, and M. E. Sullivan, "Static two-dimensional aperture coding for multimodal, multiplex spectroscopy," *Appl. Opt.*, vol. 45, no. 13, pp. 2965–2974, 2006.

[4] S. D. Feller *et al.*, "Multiple order coded aperture spectrometer," *Opt. Exp.* vol. 15, no. 9, pp. 5625–5630, 2007.

[5] C. Fernandez *et al.*, "Longwave infrared (LWIR) coded aperture dispersive spectrometer," *Opt. Exp.*, vol. 15, no. 9, pp. 5742–5753, 2007.

[6] A. W. Lohmann *et al.*, *Optical Information Processing*. Ilmenau, Germany: Ilmenau Univ., 1978.

[7] W. H. Lee, "Diffractive optics for data storage," *Proc. SPIE*, vol. 2383, pp. 390–395, May 1995.

[8] L. B. Lesem, P. M. Hirsch, and J. A. Jordan, "The kinoform: A new wavefront reconstruction device," *IBM J. Res. Develop.*, vol. 13, no. 2, pp. 150–155, Mar. 1969.

[9] F. Wyrowski and O. Bryngdahl, "Digital holography as part of diffractive optics," *Rep. Prog. Phys.*, vol. 54, no. 12, pp. 1481–1571, Dec. 1991.

[10] V. A. Soifer, *Computer Design of Diffractive Optics*. Amsterdam, The Netherlands: Elsevier, 2012.

[11] S. Banerji, M. Meem, A. Majumder, B. Sensale-Rodriguez, and R. Menon, "Imaging over an unlimited bandwidth with a single diffractive surface," 2019, *arXiv:1907.06251*. [Online]. Available: http://arxiv.org/abs/1907.06251

[12] S. Banerji and B. Sensale-Rodriguez, "A computational design framework for efficient, fabrication error-tolerant, planar THz diffractive optical elements," *Sci. Rep.*, vol. 9, no. 1, Dec. 2019, Art. no. 5801.

[13] S. Banerji *et al.*, "3D-printed diffractive terahertz optical elements through computational design," *Proc. SPIE*, vol. 10982, May 2019, Art. no. 109822X.

[14] S. F. Busch, "THz optics 3D printed with TOPAS," *J. Infr., Millim., THz Waves*, vol. 37, p. 303, Oct. 2016.

[15] E. Castro-Camus, "Additive manufacture of photonic components for the terahertz band," *J. Appl. Phys.*, vol. 127, Jun. 2020, Art. no. 210901.

[16] S. Banerji, "Imaging with flat optics: Metalenses or diffractive lenses?" *Optica*, vol. 6, pp. 805–810, Jun. 2019.

[17] S. Banerji, "Inverse designed achromatic flat lens operating in the ultraviolet," *OSA Continuum*, vol. 3, no. 7, pp. 1917–1929, 2020.

[18] S. Banerji, J. Cooke, and B. Sensale-Rodriguez, "Impact of fabrication errors and refractive index on multilevel diffractive lens performance," *Sci. Rep.*, vol. 10, no. 1, Dec. 2020, Art. no. 14608.

[19] S. F. Busch, "Optical properties of 3D printable plastics in the THz regime and their application for 3D printed THz optics," *J. Infr., Millim., THz Waves*, vol. 35, pp. 993–997, Dec. 2014.

[20] P. Wang, "Computational spectrometer based on a broadband diffractive optic," *Opt. Exp.*, vol. 22, pp. 14575–14587, Oct. 2014.

[21] J. Y. J. Yue, J. H. J. Han, Y. Z. Y. Zhang, and L. B. L. Bai, "High-throughput deconvolution-resolved computational spectrometer," *Chin. Opt. Lett.*, vol. 12, no. 4, pp. 043001–43004, 2014.

[22] P. Wang and R. Menon, "Computational spectroscopy via singular-value decomposition and regularization," *Opt. Exp.*, vol. 22, no. 18, pp. 21541–21550, 2014.

[23] B. Scherger, N. Born, C. Jansen, S. Schumann, M. Koch, and K. Wiesauer, "Compression molded terahertz transmission blaze-grating," *IEEE Trans. THz Sci. Technol.*, vol. 2, no. 5, pp. 556–561, Sep. 2012.

[24] H. Yi, S.-W. Qu, B.-J. Chen, X. Bai, K. B. Ng, and C. H. Chan, "Flat terahertz reflective focusing metasurface with scanning ability," *Sci. Rep.*, vol. 7, no. 1, Dec. 2017, Art. no. 3478.